3-Dimensional Numerical Study on the Critical Orientation of the Flooded Passenger Vehicles

Ebrahim Hamid Hussein Al-Qadami, Mohd Adib Mohammad Razi, Wawan Septiawan Damanik, Zahiraniza Mustaffa, Eduardo Martinez-Gomariz, Fang Yenn Teo, and Anwar Ameen Hezam Saeed

***Abstract*—Vehicles are one of the most common objects that are usually washed away by the water flow during flood events resulting in several damages and casualties. Regardless of the vehicle type and flow condition, vehicle orientations in relation to the incoming flow play a significant role on the vehicles stability limits. Therefore, studying the hydrodynamic forces on a vehicle placed at different angles with respect to the incoming flow can help to understand the most unstable orientation. As a result, parking lots design may improve by rearranging the vehicles in a way that the critical vehicle orientation will not face the expected incoming flow. Herein, 3-dimensional numerical modelling was conducted to assess the critical orientation of a parked full-scale passenger vehicle exposed to water flow at three different angles, namely 0^o, 45^o, and 90^o. The highest drag force and displacement were observed for the vehicle at 90^o orientation making it the critical one. While the highest torque on the vehicle centre of mass was reported for the vehicle at 45^o orientation, making it more rotatable when compared with other orientations. Obtained results were compared with previously published experimental studies and good agreements were observed.**

***Index Terms*—Floods, vehicles, numerical simulation, orientation, hydrodynamic forces**

I. Introduction

FROM long ago until nowadays, the major human settlements are mainly located along the rivers floodplain areas [1], [2], [3], [4]. The huge and rapid urbanization and development in these settlements had significantly increased the likelihood of flooding [5], [6]. Furthermore, climate change and greenhouse gas emissions (GHE) lead to many alterations in the Earth's hydrological cycle by causing more frequent floods and natural hazards [7], [8], [9]. In 2014 alone, a total of 324 natural hazards were reported around the world which affected nearly 141 million people. Floods, landslides, and waves action were 47.2% among these disasters [10]. The economic losses caused by the water-related disasters altogether in the entire World in the year 2014 were estimated to be 37.39 US billion out of which 29.42 US billion were to be borne by the continent of Asia [11]. Between 1975 and 2001, a total of 1,816 floods were reported resulted in 175,000 human casualties around the globe [12]. In East Asia, 127 flood events were reported throughout the 21^{st} century, of which 25 were categorized as flash floods and accounted for almost 30% of the total deaths. In Malaysia, the most shattering floods were reported in December 2014 and January 2015 at which more than 100,000 people were evacuated from their houses during the event [13]. More recently, the Johor flood event that occurred in January 2021 led to at least 1 death and the evacuation of 9,000 people according to Malaysia's disaster agency [14].

During flood events, vehicles are directly affected by the water flow and they may be dragged away in the flow direction once the flow velocity and water depth exceed the critical values [15], [16]. Once the vehicles become unstable, they may be dragged away causing direct damage to the properties through colliding or even causing loss of human life [17], [18]. Furthermore, flooded vehicles consequences can be made worse due to vehicles being carried out and blocking flow paths at the downstream end of the rivers. A clear example of the flooded vehicle danger was observed in the UK during the Boscastle flash flood that happened on 16 August 2004. The city was projected to an extreme flash flood caused by a heavy rainfall event up to 200 mm in 5 hours. The UK Environment Agency (2004) [19] reported that millions of pounds of damages were made and a huge agricultural land area was lost during that event. About 116 vehicles were swept away and some of them together with other large size debris were stacked under a local bridge blocking the water flow, finally causing to collapse of the bridge. Some of these vehicles were flashed out straight to the harbour without any obstruction blocks.

The main flow parameters that usually govern vehicle instability are flow velocity (v) and water depth (h). Once these parameters reach certain values, vehicles lose their instability mainly in two forms, sliding or/and floating [20]. Sliding instability mode most probably occurs at high flow velocity and low water depth (i.e., supercritical flows). On the other hand, floating instability commonly occurs at low flow velocity and high-water depth (i.e., subcritical flows) [20], [21], [22]. Besides the flow parameters, vehicles specifications and their characteristics play significant roles in determining the vehicle instability criteria [23]. These spec-

Manuscript received January 20, 2022; revised June 19, 2023.

E.H.H. Al-Qadami is a postdoctoral researcher in the Faculty of Civil Engineering & Built Environment, Universiti Tun Hussein Onn Malaysia, 86400 Parit Raja, Batu Pahat, Johor, Malaysia (email: ialgodami@gmail.com)

M. Razi is a professor in Eco Hydrology Technology Research Centre (Eco-Hytech), Faculty of Civil Engineering & Built Environment, Universiti Tun Hussein Onn Malaysia, 86400 Parit Raja, Batu Pahat, Johor, Malaysia (email: adib@uthm.edu.my)

W. S. Damanik is a lecturer in the Department of Mechanical Engineering, Universitas Muhammadiyah Sumatera Utara Jl.Mukhtar Basri No.3 Medan-North Sumatera, Indonesia (email: wawanseptiawan@umsu.ac.id)

Z. Mustaffa is an associate professor in Universiti Teknologi PETRONAS, Department of Civil and Environmental Engineering, Seri Iskandar, Perak, Malaysia (email: zahiraniza@utp.edu.my)

E. Martinez-Gomariz is a research fellow at Flumen Research Institute. Universitat Politcnica de Catalunya, Barcelona, Spain (email: eduardo.martinez-gomariz@upc.edu)

F. Teo is an associate professor in the Department of Civil Engineering, University of Nottingham, Semenyih 43500, Malaysia (email: fangyenn.teo@nottingham.edu.my)

A. A. H. Saeed is a postdoctoral researcher in the Chemical Engineering Department, Universiti Teknologi PETRONAS, Bandar Seri Iskandar 32610, Perak, Malaysia (Email: anwar_17006829@utp.edu.my)

ifications are i) vehicle dimensions (length, width, height, and ground clearance) ii) vehicle weight, iii) vehicle external hydrodynamic design, and iv) tires conditions (old/new), and v) ground surface conditions [22]. Furthermore, vehicle orientation with respect to the flow direction has a major effect on vehicles instability [24], [25], [26].

During the past years, few numerical studies have been conducted to investigate the vehicles instabilities during flood events. In most cases, using numerical approaches gives more detailed results when compared with the experimental runs. However, the previous numerical studies were not conducted under six degrees of freedom which makes them not exactly represent the real experiments. Xia et al., (2011) [27] carried out a numerical study to assess flood hazard risk to both vehicles and people during flood events using an existing 2D hydrodynamic model. A hazard degree (HD) expression was introduced and used to quantify the corresponding degree of hazard. Based on HD, vehicles were considered to be safe if HD = 0, namely, U $<<$ Uc, while vehicles were considered to be unsafe if HD approached 1.0, namely, U $\geq$ Uc, where U and U_c are the flow and critical flow velocities respectively. Later in 2015, Arrighi et al., (2015) [28] investigated the vehicle instability modes numerically using the computational fluid dynamics (CFD) toolbox in OpenFOAM. A mobility parameter (θ_v) was introduced to describe vehicles instability modes as a function of Froude's number.

In this study, a 3-dimensional numerical modelling was conducted to assess the critical orientation of a full-scale passenger vehicle during flood events. The numerical runs considered six degrees of freedom and coupled motion to represent the real conditions. First, in this paper a detailed description of the methodology is presented, including geometries creation, selected boundary and initial conditions, mesh development, and general numerical setup. Second, results are presented and discussed in terms of water flow condition, hydrodynamic forces, torque, and flow patterns. Later, a comparison between the presented results and previously published experimental investigations are introduced. Finally, some conclusions are presented and summarized at the end of the paper.

II. Methodology

In this study, the science of computational fluid dynamics (CFD) was used to investigate the critical vehicle orientation in flooding. Among available commercial CFD software, FLOW-3D that uses finite volume method (FVM) and turbulence models to solve the Reynolds-Averaged Navier-Stokes (RANS) equations [29], [30], [31] was selected to conduct the numerical runs. FLOW-3D was used because it has the advantage of built-in six degrees of freedom and coupled motion simulation tools [32]. A total of three vehicle orientations were tested namely (i) 0^o, at which the vehicle front side was facing the incoming flow, (ii) 45^o, at which the vehicle was rotated (45^o) with the direction of the incoming flow, and (iii) 90^o, at which the vehicle longitudinal side was facing incoming flow as shown in Figs. 1a, 1b, and 1c, respectively.

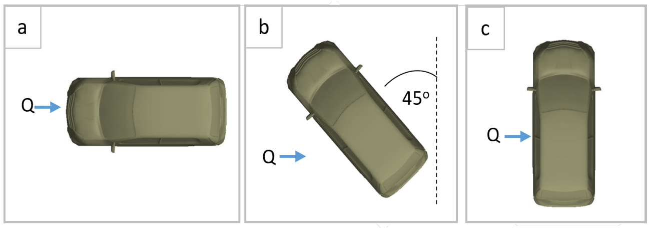

Fig. 1. Vehicle orientations against the incoming flow (a) 0^o, (b) 45^o, and (c) 90^o, (owned by authors)

A. Meshing and geometry

Herein, a full-scale medium-size Malaysian passenger vehicle called Perodua Viva was used to conduct the numerical runs. The 3D geometry model of the vehicle was developed using Solidworks then converted to STL format to be inserted into FLOW-3D software. The vehicle model was placed on a rectangular plate with dimensions of 12 m length, 10 m width, and 0.2 m height. The plate was considered as the road and its surface roughness was defined with a static friction coefficient of 0.3. Two mesh blocks (containing and nested) were developed to contain both the fluid and solid domains as shown in Figs. 2a-2c. The nested mesh block was developed with a cell size of 0.025 m to accurately capture the vehicle geometry model, while the containing mesh block cell size was 0.05 m. Table 1 shows a detailed description of the mesh arrangement used in this study. Before conducting numerical runs, the mesh quality was checked by running the FAVOR solver, and it was noticed that the selected mesh cell sizes were accurately captured both fluid and solid domains as shown in Fig. 3. One history probe was placed 3 m ahead of the vehicle location (Fig. 2) to measure the flow variables such as velocity, depth, and Froude's number. The boundary conditions for all the cases were the same (Fig. 2) for the purpose of conducting a comparison between the cases in terms of forces and stability conditions. The inlet boundary was defined with flow velocity and water depth, while the outlet boundary was defined as a free-fall with atmospheric pressure and 0 fluid fractions. The top faces of both containing and nested mesh blocks were defined as free surface flow with atmospheric pressure and 0 fluid fractions. The rest of the sides were defined as walls for the containing mesh block and symmetry for the nested mesh block as shown in Fig. 2.

B. Governing equations

Fluid flow governing equations including mass continuity and momentum equations were solved numerically to simulate the flow in a 3D form. These equations can be written in a general form as in Equations 1-4 respectively.

$$V_F\frac{\partial \rho}{\partial t}+\frac{\partial}{\partial x}(\rho u A_x)+R\frac{\partial}{\partial y}(\rho v A_y)+\frac{\partial}{\partial z}(\rho w A_z)+\xi\frac{\rho u A_x}{x}=R_{\mathrm{DIF}}+R_{\mathrm{SOR}} \quad (1)$$

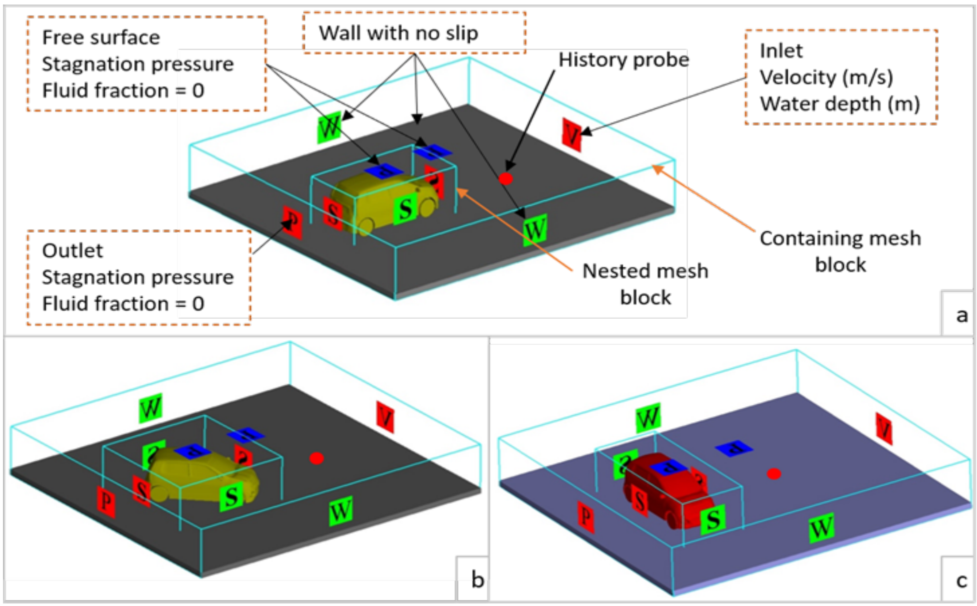

Fig. 2. Boundary conditions and mesh blocks arrangement (a) 0^o, (b) 45^o, and (c) 90^o

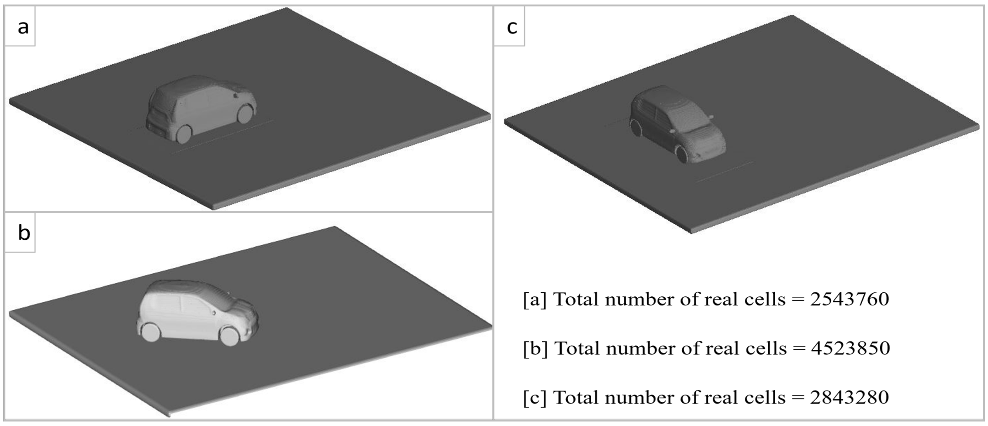

Fig. 3. Geometries visualization after running FAVOR solver (a) 0^o, (b) 45^o, and (c) 90^o

TABLE I
DETAILS OF THE GENERATED MESH BLOCKS

Vehicle orientation	0^o		45^o		90^o	
Mesh block	Containing	Nested	Containing	Nested	Containing	Nested
Cells size (m)	0.05	0.025	0.05	0.025	0.05	0.025
Cells number	1,576,080	967,680	1,576,080	3,618,000	1,576,080	1,267,200
Domain	Fluid and vehicle	Vehicle	Fluid and vehicle	Vehicle	Fluid and vehicle	Vehicle

$$\frac{\partial u}{\partial t}+\frac{1}{V_F}\left\{uA_x\frac{\partial u}{\partial x}+vA_yR\frac{\partial u}{\partial y}+wA_z\frac{\partial u}{\partial z}\right\}-\xi\frac{A_yv^2}{xV_F} = -\frac{1}{\rho}\frac{\partial p}{\partial x}+G_x+f_x-b_x-\frac{R_{\mathrm{SOR}}}{\rho V_F}(u-u_w-\delta u_s) \quad (2)$$

$$\frac{\partial v}{\partial t}+\frac{1}{V_F}\left\{uA_x\frac{\partial v}{\partial x}+vA_yR\frac{\partial v}{\partial y}+wA_z\frac{\partial v}{\partial z}\right\}+\xi\frac{A_yuv}{xV_F} = -\frac{1}{\rho}\left(R\frac{\partial p}{\partial y}\right)+G_y+f_y-b_y-\frac{R_{\mathrm{SOR}}}{\rho V_F}(v-v_w-\delta v_s) \quad (3)$$

$$\frac{\partial w}{\partial t}+\frac{1}{V_F}\left\{uA_x\frac{\partial w}{\partial x}+vA_yR\frac{\partial w}{\partial y}+wA_z\frac{\partial w}{\partial z}\right\} = -\frac{1}{\rho}\frac{\partial p}{\partial z}+G_z+f_z-b_z-\frac{R_{\mathrm{SOR}}}{\rho V_F}(w-w_w-\delta w_s) \quad (4)$$

where, V_F is the fractional volume open to flow, ρ is the fluid density, (u, v, w) are the velocity components in the coordinate directions (x, y, z) or (r, θ, z), (A_x, A_y, A_z) are the fractional area open to flow in the (x, y, z) directions, respectively, R_{SOR} is the density source term, R_{DIF} is the turbulence diffusion term, R and ξ are the coefficients depend on the coordinate system. When cylindrical coordinates are used, y derivatives must be converted to azimuthal derivatives, and ξ set to be 1. When Cartesian coordinates are to be used, R is set to unity and ξ is set to zero, (G_x, G_y, G_z) are the body accelerations, (f_x, f_y, f_z) are viscous accelerations, (b_x, b_y, b_z) are flow losses in porous media or across porous baffle plates, the final terms account for the injection of mass at a source represented by a geometry, and p is the pressure.

The turbulence flow was solved by enabling the two-equation $K-\epsilon$ model (turbulent kinetic energy k_T (Equation 5), and its dissipation ϵ_T (Equation 6)) which is commonly considered as a sophisticated and more widely used model that provides a stable numerical simulation.

$$\frac{\partial k_T}{\partial t} + \frac{1}{V_F}\left\{uA_x\frac{\partial k_T}{\partial x} + vA_y\frac{\partial k_T}{\partial y} + wA_z\frac{\partial k_T}{\partial z}\right\} = P_T + G_T + \mathrm{Diff}_{k_T} - \varepsilon_T \quad (5)$$

$$\frac{\partial \varepsilon_T}{\partial t} + \frac{1}{V_F}\left\{uA_x\frac{\partial \varepsilon_T}{\partial x} + vA_yR\frac{\partial \varepsilon_T}{\partial y} + wA_z\frac{\partial \varepsilon_T}{\partial z}\right\} = \frac{\mathrm{CDIS1}\cdot\varepsilon_T}{k_T}(P_T + \mathrm{CDIS3}\cdot G_T) + \mathrm{Diff}_\varepsilon - \mathrm{CDIS2}\frac{\varepsilon_T^2}{k_T} \quad (6)$$

Where V_F, A_x, A_y, and A_z are FLOW-3Ds FAVOR solver functions, P_T is the turbulent kinetic energy production, $CDIS1, CDIS2$, and $CDIS3$ are dimensionless user-adjustable parameters, and have defaults of 1.44, 1.92 and 0.2, respectively, and $\mathrm{Diff}_\varepsilon$ is the diffusion of dissipation.

As mentioned previously that this study was conducted under the six degrees of freedom condition, thus the rigid-body equations of motion, as well as the rigid-body dynamic equations (collision model), were enabled and solved. Transitional and rotational governing equations of motion can be written as in Equations 7 and 8. On the other hand, the collision model was simulated by solving equations 9-11.

$$F = m\frac{dV_G}{dt} \quad (7)$$

$$\mathbf{T}_G = [J]\cdot\frac{d\omega}{dt} + \omega\times([J]\cdot\omega) \quad (8)$$

$$\sqrt{(dp_1)^2 + (dp_2)^2} < \mu\, dp \quad \textbf{if} \quad {v_1}^2 + {v_2}^2 = 0 \quad (9)$$

$$dp_i = -\frac{\mu\, v_i}{\sqrt{{v_1}^2 + {v_2}^2}}dp \quad \mathbf{i = 1, 2,} \quad \textbf{if} \quad {v_1}^2 + {v_2}^2 = 0 \quad (10)$$

$$e = \sqrt{-\frac{W_3(p_f) - W_3(p_c)}{W_3(p_c)}} \quad (11)$$

where, F is the total force, m is rigid body mass, T_G is the total torque about G, and $[J]$ is moment of inertia tensor in the body system, W_3 is work done by normal impulse, p_c is the normal impulse when collision reaches maximum compression, and p_f is the total impulse of collision. Restitution coefficient ranged between 0 and 1, where 0 represents perfect inelastic collision, 1 represents perfect elastic collision. Values between 0 and 1 represent partially elastic collision.

III. Results and Discussion

The different hydrodynamic forces and the responses of a passenger vehicle at three different orientations (0^o, 45^o, and 90^o) are presented here. Figs. 4a to 4c show the variation of flow depth, flow velocity, and Froude number with time, respectively. All these variables were extracted from the history probe that was placed 3 m ahead of the vehicle location. In general, the same pattern of flow behaviour was noticed for all vehicle orientations, which provides a good indication of the numerical setup and the selected boundary conditions. From Figs. 4a to 4c, it can be noticed that the simulation reached the steady-state after 16 seconds at which there were no major changes in the flow parameters values. A minor variation in the flow velocity in the case of 90^o orientation was observed. This could be due to the back-flow effects that was generated after the flow hit the vehicle's longitudinal side.

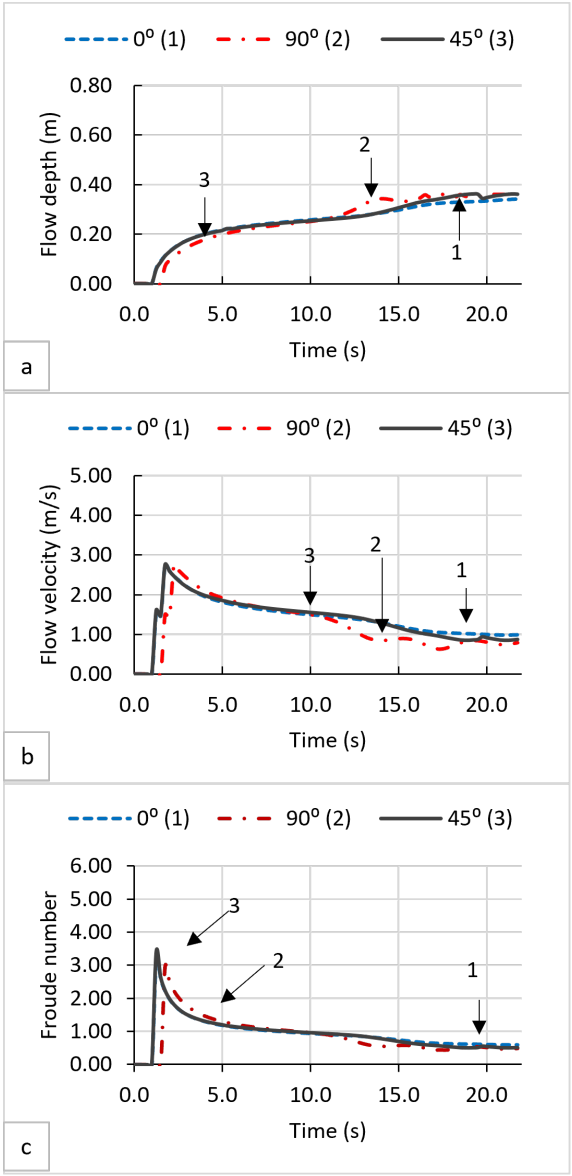

Fig. 4. Flow variables change with time at 3 m ahead of the vehicle

Figs. 5a to 5c illustrate the variation of the pressure forces with time in the x, y, and z directions, respectively. It was observed that the x-pressure force that acts in parallel with the flow direction was the highest for vehicle orientation of 90^o with an average value of 1,242 N. For 0^o vehicle orientation, the x-pressure force was the lowest with an average value of 447 N. The x-pressure force for 45^o vehicle orientation was between both previously mentioned values with an average magnitude of 961 N as shown in Fig. 5a. It can be clearly noticed that magnitude of the pressure forces was proportionally changed with the affected vehicle area. On the other hand, the y-pressure force was the highest at 45^o vehicle orientation as shown in Fig. 5b with an average value of 456 N. However, the y-pressure force was almost equal to 0 for other vehicle orientations (0^o and 90^o). This was because the normal projected area to the y-direction was in parallel with the flow direction for both orientations.

The resultant horizontal force that causes the sliding instability mode was calculated for 45^o vehicle orientation. The resultant force calculated from both x and y-pressure forces for 45^o vehicle orientation was found to be 1,063 N. When comparing the resultant horizontal force on the vehicle at 45^o orientation (R= 1,063 N) with the other horizontal forces (F_H= 1,242 for 90^o, and F_H= 447 N for 0^o) it can be noticed that highest horizontal drag force was recorded at 90^o vehicle orientation. It can be concluded that the critical vehicle orientation was when the vehicle's longitudinal side was facing the incoming flow. Fig. 5c shows the vertical pressure forces variation with time for all simulated vehicle orientations. The vertical pressure forces were almost the same for all cases, however, the highest value was observed for the vehicle at 0^o vehicle orientation. This was due to the effects of the size of the projected area of the tiers with respect to the incoming flow. For 0^o vehicle orientation, the projected tires area is less when compared with other vehicle orientations.

As previously mentioned, all numerical runs were conducted under six degrees of freedom and coupled motion. Thus, the difference between the initial and final of the vehicle centre of mass was calculated. In general, the vehicle was observed to be stable under the selected flow velocity and water depth at the inlet boundary. However, a very minor difference was observed, this can also confirm or provide an indication regarding the critical vehicle orientation. From Table 3, it can be noticed that the highest displacement was observed at 90^o vehicle orientation with a total displacement of 0.015 m in the x-direction. On the other hand, the displacement for other vehicle orientations (0^o and 45^o) were 0 and 0.008, respectively. It can also be noticed that the displacements in the z-direction were 0 for all vehicle orientations due to the low water depth at the vehicle vicinity.

TABLE II
DISPLACEMENTS OF THE VEHICLE CENTRE OF MASS

Vehicle orientation	Displacement (m)		
	x	y	z
0^o	0.005	0.000	0.000
45^o	0.008	0.001	0.000
90^o	0.015	0.000	0.000

Fig. 6 shows the variation of the torque about the vehicle centre of mass variation with time. Unexpectedly, it was observed that the magnitude of the torque for the vehicle at 0^o orientation was more than the torque magnitude for

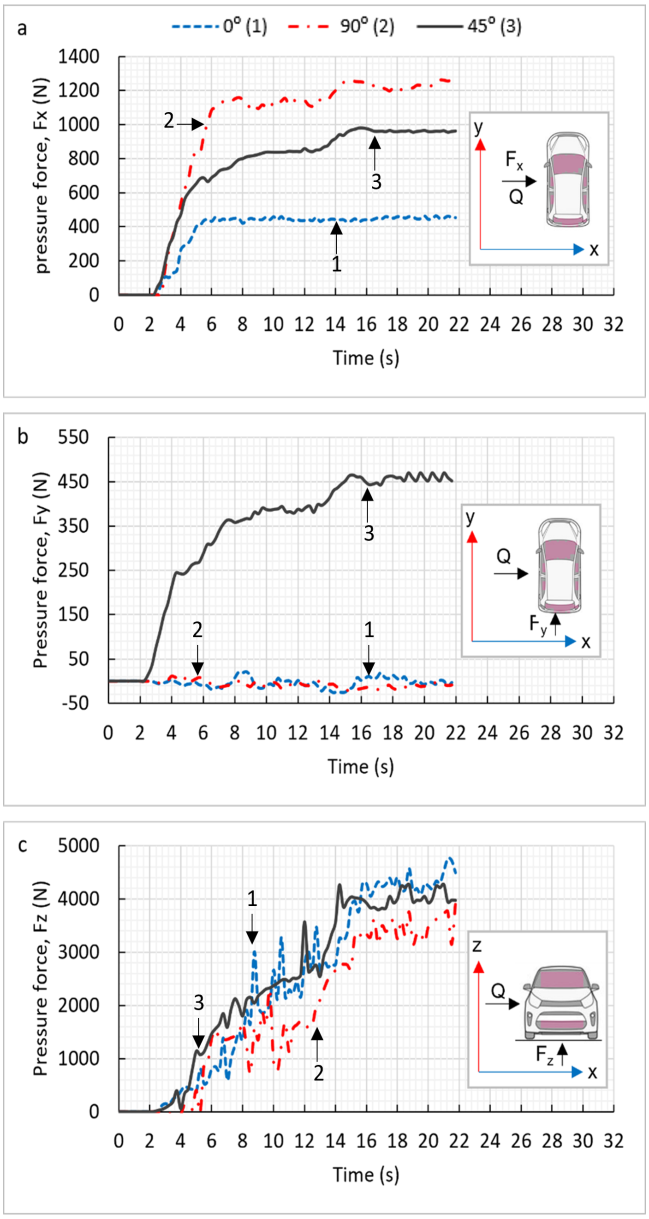

Fig. 5. Pressure forces variation with time (a) x direction, (b) y direction, (c) z direction

the vehicle at 90^o orientation. On the other side, the highest torque magnitude was observed for vehicle orientations of 45^o as shown in Fig. 6. This indicated that the vehicle parked at 45^o with respect to the incoming flow tended to be more rotated due to the flow velocity.

For a better understanding of the flow behaviour at the vehicle vicinity, 2D renderings of the flow velocity, streamlines, Froude number, and water depth were extracted for all studied cases and are presented in Figs. 7a, 7b, 8a, and 8b, respectively. The lowest flow velocities and the highest water depths were observed at the vehicles sides that were facing the incoming flow as well as behind the tires. Furthermore, it was observed that the flow velocity was low ahead of the vehicle locations, however, the flow velocity was higher after the vehicle locations for all simulated orientations. On the other hand, the vice versa was observed for the flow depth before and after the vehicle location. In terms of Froude number, it can be seen that once the flow hit the vehicle body it reached to the lowest value, while its magnitude increased

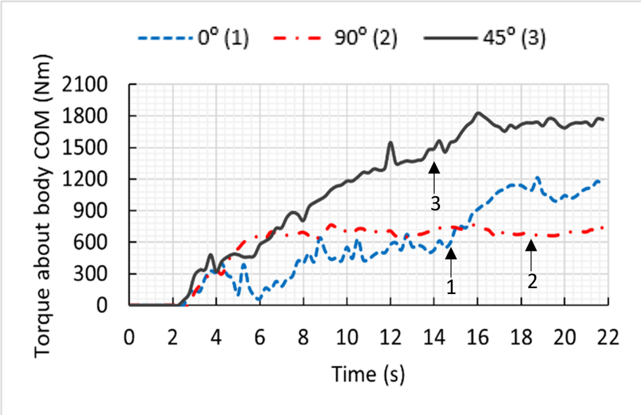

Fig. 6. Torque about the vehicle centre of mass variation with time

once the flow passed the vehicle body. Besides, it can be noticed that the vehicle's tires minimize the Froude number to its lowest especially at vehicle orientations of 90^o and 45^o (Fig. 8a).

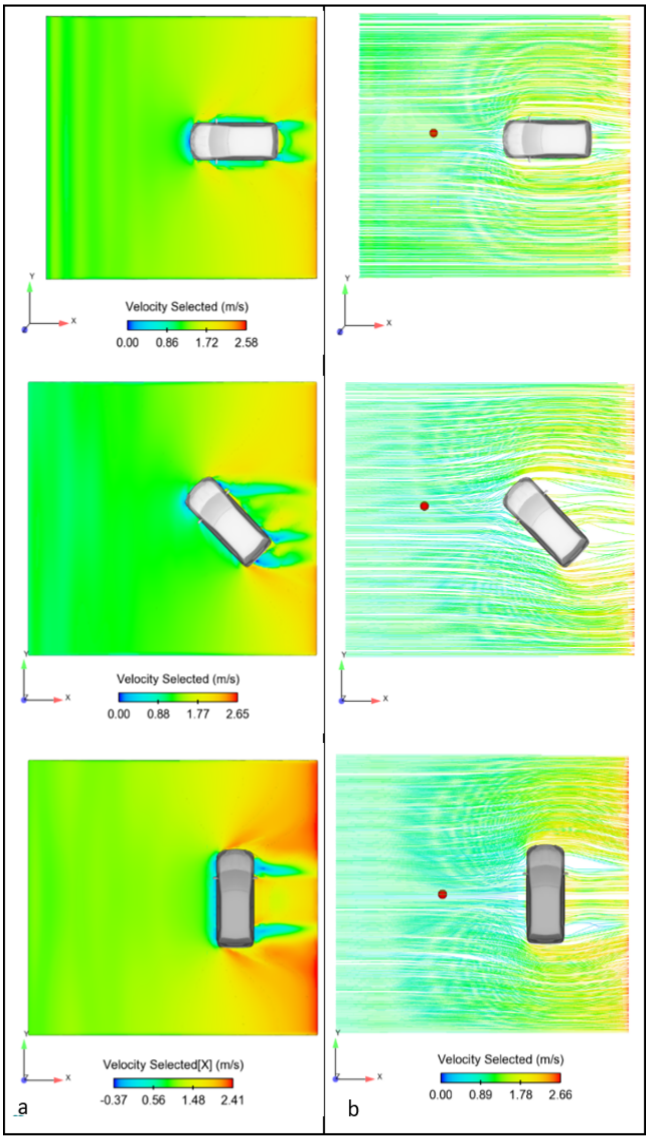

Fig. 7. 2D rendering (a) flow velocity, and (b) streamlines

Fig. 9 shows a 3D rendering for the flow velocity at which

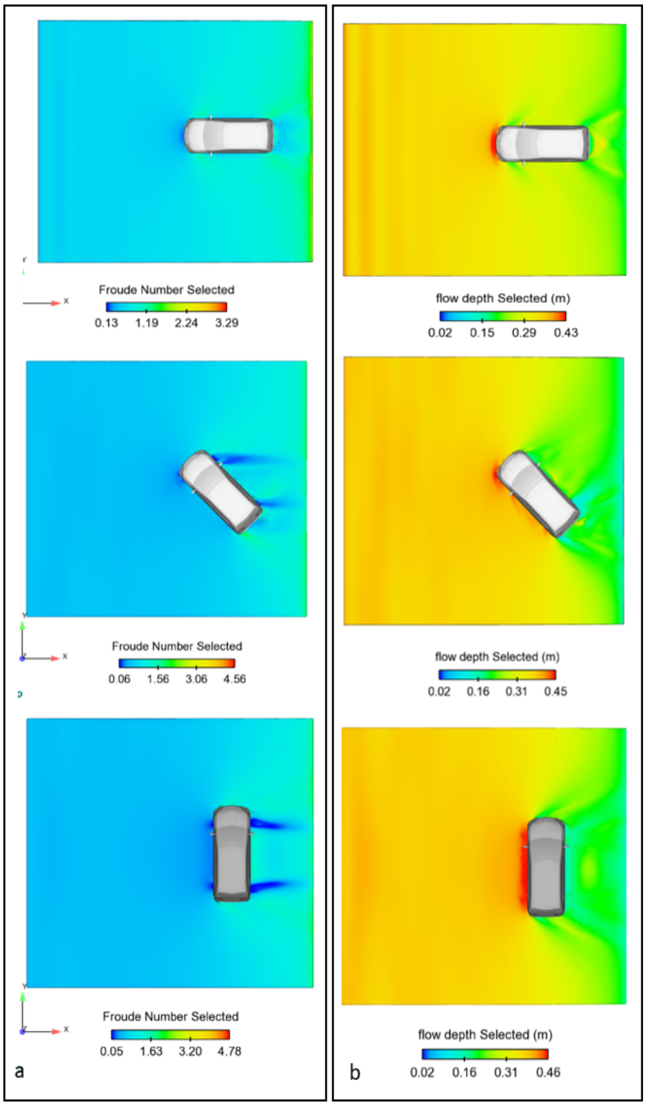

Fig. 8. 2D rendering (a) Froude number, and (b) water depth

the vehicle longitudinal side was facing the incoming flow (90^o). The 3D rendering provides a better visualization on the flow pattern and describes the flow velocity magnitudes at each point around the vehicle body. It can be noticed that the flow velocity is the lowest behind the vehicle's tires (locations 1 and 2) at which the flow was blocked. While the velocity was the highest at location 3 where the flow passed underneath the vehicle.

IV. Validation

The obtained results from this study were compared with the previously published experimental works. Herein, two different experimental studies were considered including (i) Shah et. al. (2018) [33], and (ii) Al-Qadami et. al. (2021) [20].

A. *Shah et. al. (2018) [33]*

Shah et. al. (2018) [33] conducted a series of experimental runs to investigate the stability limits of a passenger vehicle called Volkswagen Scirocco R at a scale of 1:24. Different vehicle orientations with respect to the incoming flow were considered, including 0^o, 45^o, 90^o, 135^o, 180^o, 225^o, 270^o,

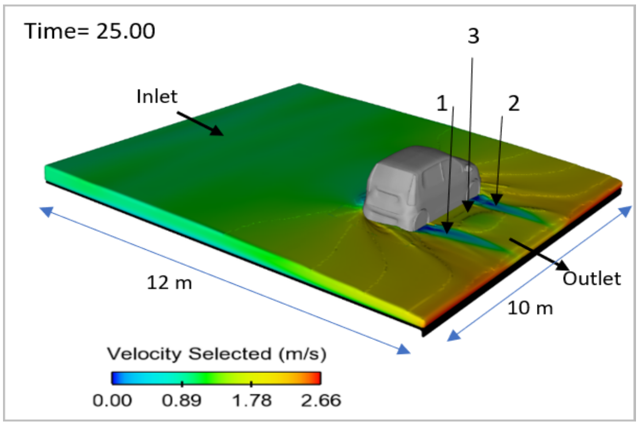

Fig. 9. 3D rendering of flow velocity for vehicle orientation of (90^o)

315^o, and 360^o. The $depth \times velocity$ (d*v) function was obtained for all orientations. It was noticed that for the vehicle at 0^o (front end facing flow direction) and 360^o (rear end facing flow direction) orientations, the d*v was 0.0168 m^2/s, while it was 0.0156 m^2/s for the vehicle at 45^o orientation. On the other hand, at 90^o orientation (side part facing flow direction), the d*v was 0.0144 m^2/s. Based on the outcomes it was concluded that the vehicle at 90^o was critical when compared with other orientations. These outcomes are in agreement with the findings obtained numerically in this study.

B. Al-Qadami et. al. (2021) [20]

Al-Qadami et. al. (2021) [20] investigated the stability of a full-scale medium size Malaysian passenger vehicle inside floodwaters experimentally. Experimental runs were conducted in a 10 m wide laboratory tank under various flow depths, velocities, and orientations (0^o, and 90^o). Sliding instability mode was proposed to occur when the drag force is equal to or greater than the friction force ($F_D \geq F_R$). It was reported that the hydrodynamic forces on the vehicle at 90^o orientation were higher when compared with 0^o under same flow condition. Therefore, according to Al-Qadami et. al. (2021) [20] the critical vehicle orientation is 90^o at which the vehicle longitudinal side is facing the incoming flows. These observations were found to be in agreement with the numerical results presented in this study.

V. Conclusion

In this study, a 3-dimensional numerical modelling integrated with six degrees of freedom and coupled motion tools was conducted to assess the critical orientation of a full-scale passenger vehicle parked on a flooding plain. Three different vehicle orientations were simulated, namely 0^o, 45^o, and 90^o. The vertical and horizontal hydrodynamic forces that acted on the vehicle sides were recorded at each time step. Results showed that the highest horizontal force was on the vehicle at 90^o orientation with an average value of 1,242 N. On the other hand, the horizontal forces that acted on the 0^o and 45^o vehicle orientations were 447 N and 1,063 N, respectively. Furthermore, the highest horizontal displacement of the vehicle center of mass was 0.015 m which was reported for the vehicle at 90^o orientation. In terms of torque measurements, it was noticed that the highest torque value was recorded for the vehicle at 45^o orientation. According to these observations, it can be concluded that the critical vehicle orientation in terms of sliding instability mode is 90^o at which the vehicle longitudinal side was facing the incoming flow. On the other hand, the vehicle tends to be more rotatable at the orientation of 45^o. Therefore, it is recommended that the arrangement of the vehicle in parking lots should be in a way that the vehicle's longitudinal side will not face the incoming flow, and ensure that the incoming flow only face the vehicle front or rear sides. For the future studies, it is recommended to conduct the numerical runs using different vehicle models especially those once used for evacuation during flood events such as ambulance, police, fire vehicles.

References

[1] D. Aithani, D. S. Jyethi, Z. Siddiqui, A. K. Yadav, and P. Khillare, "Source apportionment, pollution assessment, and ecological and human health risk assessment due to trace metals contaminated groundwater along urban river floodplain." *Groundwater for Sustainable Development*, vol. 11, pp. 100 445–100 459, 2020.

[2] M. S. B. Khalid and S. B. Shafiai, "Flood disaster management in malaysia: An evaluation of the effectiveness flood delivery system," *International Journal of Social Science and Humanity*, vol. 5, no. 4, pp. 398–402, 2015.

[3] K. Li, W. Gao, L. Wu, H. Hu, P. Gong, S. Li, R. Jin, and Y. Si, "Spatial expansion of human settlement during the longshan period (˜ 4.5–˜ 3.9 ka bp) and its hydroclimatic contexts in the lower yellow river floodplain, Eastern China," *Land*, vol. 10, no. 7, pp. 712–718, 2021.

[4] R. A. Falconer, B. Lin, and J. Xia, "2d hydrodynamic modelling: Mobile beds, vehicle stability and severn estuary barrage," *FRMRC Food Risk Management Research Consortium*, pp. 1–33, 2012.

[5] M. Shao, G. Zhao, S.-C. Kao, L. Cuo, C. Rankin, and H. Gao, "Quantifying the effects of urbanization on floods in a changing environment to promote water securitya case study of two adjacent basins in texas," *Journal of Hydrology*, vol. 589, pp. 125 154–125 167, 2020.

[6] S. Bae and H. Chang, "Urbanization and floods in the seoul metropolitan area of south korea: What old maps tell us," *International Journal of Disaster Risk Reduction*, vol. 37, pp. 101 186–101 197, 2019.

[7] O. Ivanova, A. Aleksandrov, and R. Revetria, "Modelling of impact caused by flood after water flow optimization at volga-kama river basin." *Engineering Letters*, vol. 27, no. 4, pp. 658–662, 2019.

[8] S. M. H. Shah, Z. Mustaffa, F. Y. Teo, M. A. H. Imam, K. W. Yusof, and E. H. H. Al-Qadami, "A review of the flood hazard and risk management in the south asian region, particularly pakistan," *Scientific African*, pp. e00 651–e00 670, 2020.

[9] J. Thistlethwaite, A. Minano, J. A. Blake, D. Henstra, and D. Scott, "Application of re/insurance models to estimate increases in flood risk due to climate change," *Geoenvironmental Disasters*, vol. 5, no. 1, pp. 1–13, 2018.

[10] B. B. Walker, C. Taylor-Noonan, A. Tabbernor, T. McKinnon, H. Bal, D. Bradley, N. Schuurman, and J. J. Clague, "A multi-criteria evaluation model of earthquake vulnerability in victoria, british columbia," *Natural hazards*, vol. 74, no. 2, pp. 1209–1222, 2014.

[11] S. M. H. Shah, Z. Mustaffa, and K. W. Yusof, "Disasters worldwide and floods in the malaysian region: a brief review," *Indian Journal of Science and Technology*, vol. 10, no. 2, pp. 1–9, 2017.

[12] S. Jonkman and E. Penning-Rowsell, "Human instability in flood flows 1," *JAWRA Journal of the American Water Resources Association*, vol. 44, no. 5, pp. 1208–1218, 2008.

[13] T. S. Aisha, S. Wok, A. M. A. Manaf, and R. Ismail, "Exploring the use of social media during the 2014 flood in malaysia," *Procedia-Social and Behavioral Sciences*, vol. 211, pp. 931–937, 2015.

[14] M. W. A. Ramli, N. E. Alias, H. Mohd Yusof, Z. Yusop, and S. M. Taib, "Development of a local, integrated disaster risk assessment framework for malaysia," *Sustainability*, vol. 13, no. 19, pp. 10 792–10 814, 2021.

[15] E. H. Hussein Al-Qadami, Z. Mustaffa, A. S. Abdurrasheed, H. Takaijudin, S. M. Hussain Shah, and K. W. Yusof, "Static and moving vehicles stability criteria inside floodwaters-a review." *Engineering Letters*, vol. 29, no. 3, pp. 264–1276, 2021.

[16] Z. Mustaffa, E. H. H. Al-Qadami, S. M. H. Shah, and K. W. Yusof, "Impact and mitigation strategies for flash floods occurrence towards vehicle instabilities," in *Flood Impact Mitigation and Resilience Enhancement*, pp. 1–19.

[17] S. M. H. Shah, Z. Mustaffa, E. Martínez-Gomariz, K. W. Yusof, and E. H. H. Al-Qadami, "A review of safety guidelines for vehicles in floodwaters," *International Journal of River Basin Management*, vol. 19, no. 1, pp. 25–41, 2021.

[18] S. M. H. Shah, Z. Mustaffa, E. Matínez-Gomariz, K. W. Yusof, and E. H. H. Al-Qadami, "Hazard risks pertaining to partially submerged non-stationary vehicle on low-lying roadways under subcritical flows," *Results in Engineering*, vol. 3, pp. 100 032–10 043, 2019.

[19] C. Fenn, R. Bettess, B. Golding, F. Farquharson, and T. Wood, "The boscastle flood of 16 august 2004: Characteristics, causes and consequences," pp. 1–12, 2005.

[20] E. H. H. Al-Qadami, Z. Mustaffa, S. M. H. Shah, E. Matínez-Gomariz, and K. W. Yusof, "Full-scale experimental investigations on the response of a flooded passenger vehicle under subcritical conditions," *Natural Hazards*, pp. 1–24, 2021.

[21] E. H. Al-Qadami, Z. Mustaffa, A. S. Abdurrasheed, W. Khamaruzaman, S. Shah, M. Malek *et al.*, "Numerical assessment on floating stability limits for static vehicle under partial submergence," *Journal of Engineering Science and Technology*, vol. 15, no. 2, pp. 1384–1398, 2020.

[22] E. Martínez-Gomariz, M. Gómez, B. Russo, and S. Djordjević, "A new experiments-based methodology to define the stability threshold for any vehicle exposed to flooding," *Urban Water Journal*, vol. 14, no. 9, pp. 930–939, 2017.

[23] E. Martinez-Gomariz, M. Gomez, B. Russo, and S. Djordjević, "Stability criteria for flooded vehicles: A state-of-the-art review," *Journal of Flood Risk Management*, vol. 11, pp. S817–S826, 2018.

[24] C. Arrighi, F. Castelli, and H. Oumeraci, "Effects of flow orientation on the onset of motion of flooded vehicles," *Sustainable hydraulics in the era of global change*, pp. 837–841, 2016.

[25] J. Xia, R. A. Falconer, X. Xiao, and Y. Wang, "Criterion of vehicle stability in floodwaters based on theoretical and experimental studies," *Natural hazards*, vol. 70, no. 2, pp. 1619–1630, 2014.

[26] K. Toda, T. Ishigaki, and T. Ozaki, "Experiments study on floating car in flooding," in *International Conference on Flood Resilience: Experiences in Asia and Europe*, vol. 6, 2013, pp. 1–33.

[27] J. Xia, R. A. Falconer, B. Lin, and G. Tan, "Modelling flash flood risk in urban areas," in *Proceedings of the Institution of Civil Engineers-Water Management*, vol. 164, no. 6. Thomas Telford Ltd, 2011, pp. 267–282.

[28] C. Arrighi, J. Alcèrreca-Huerta, H. Oumeraci, and F. Castelli, "Drag and lift contribution to the incipient motion of partly submerged flooded vehicles," *Journal of Fluids and Structures*, vol. 57, pp. 170–184, 2015.

[29] A. Abdurrasheed, K. Yusof, H. Takaijudin, E. Al-Qadami, A. Ghani, M. Muhammad, A. Sholagberu, V. Kumar, and S. Patel, "An integrated technique for assessing flow parameters through subsurface drainage module systems," in *IOP Conference Series: Earth and Environmental Science*, vol. 476, no. 1. IOP Publishing, 2020, pp. 012 112–012 126.

[30] S. Abdurrasheed, K. Wan Yusof, E. Hamid Hussein Alqadami, H. Takaijudin, M. M. Muhammad, A. T. Sholagberu, M. K. Zainalfikry, M. Osman, M. Shihab Patel *et al.*, "Modelling of flow parameters through subsurface drainage modules for application in bioecods," *Water*, vol. 11, no. 9, pp. 1823–1837, 2019.

[31] E. H. H. Al-Qadami, A. S. Abdurrasheed, Z. Mustaffa, K. W. Yusof, M. Malek, and A. Ab Ghani, "Numerical modelling of flow characteristics over sharp crested triangular hump," *Results in Engineering*, vol. 4, pp. 100 052–100 063, 2019.

[32] E. H. H. Al-Qadami, Z. Mustaffa, E. Martínez-Gomariz, K. W. Yusof, A. S. Abdurrasheed, and S. M. H. Shah, "Numerical simulation to assess floating instability of small passenger vehicle under subcritical flow," in *Proceedings of the International Conference on Civil, Offshore and Environmental Engineering*. Springer, 2021, pp. 258–265.

[33] S. M. H. Shah, Z. Mustaffa, and K. W. Yusof, "Experimental studies on the threshold of vehicle instability in floodwaters," *Jurnal Teknologi*, vol. 80, no. 5, pp. 25–36, 2018.